How to cite: *Angew. Chem. Int. Ed.* **2025**, *64*, e202511936
doi.org/10.1002/anie.202511936

Anion Channels **Hot Paper**

Dual-Function Tetrabenzylphosphonium Groups as Mitochondria-Targeting Artificial Anion Channels

Fei Gou⁺, Xinlei Huangfu⁺, Qiuting Wang, Zihong Yang, Xiyu Yuan, Wenju Chang, Jie Shen, Wen-Xiong Zhang,* and Huaqiang Zeng**

Abstract: Artificial ion channels with specific organelle-targeting capabilities have been scarcely investigated. Here, we report the first-in-class mitochondria-targeting anion channels derived from a structurally simple tetrabenzylphosphonium framework, in stark contrast to its phenyl-based counterpart, which lacks anion transport activity. Structural and computational analyses underscore the critical role of the methylene (CH_2) linkers in the benzyl groups. These CH_2 units reduce positive charge delocalization to enhance σ-hole–anion interactions, while also enabling H-atoms from both the CH_2 linkers and aromatic rings to cooperatively form multiple C─H···anion H─bonds. In further conjunction with the rigid benzene rings, they help create sufficient spatial voids to accommodate anion translocation, collectively facilitating and energizing the anion transport process. Among the series studied, those bearing methyl and *tert*-butyl substituents exhibit the highest transport activity via a channel mechanism, with a conductance value as high as 26.5 ± 0.8 pS. Furthermore, leveraging the cationic nature of the quaternary phosphonium center, this family of anion channels readily achieves targeted mitochondrial localization, demonstrating potent anticancer activity, with IC_{50} values ranging from 1.42 to 3.04 μM across three cancer cell lines.

The transmembrane transport of anions (e.g., Cl^-, HCO_3^-, NO_3^-) plays a vital role in maintaining cellular homeostasis, regulating acid—base balance, controlling cell volume, facilitating neuronal signalling, and supporting metabolite transport.[1–2] The directional flow of Cl^-, primarily mediated by the cystic fibrosis transmembrane conductance regulator (CFTR), is essential for fluid secretion and absorption.[3–6] Meanwhile, HCO_3^- transport is critical for intracellular pH regulation and carbon dioxide transport.[7–9] Importantly, disruptions in anion transport are directly associated with diseases such as cystic fibrosis, congenital myotonia, and renal tubular acidosis.[1] Systematic studies of natural anion transport proteins (e.g., CFTR, ClC, AE1) reveal that these protein families have evolved highly ordered 3D structures, leveraging noncovalent interactions—electrostatic forces, H─bonds, ion-dipole effects and hydrophobic interactions—to achieve efficient and selective anion transport under dynamic regulatory mechanisms, including voltage gating, ligand gating, or pH responsiveness.[10–12]

To emulate the functions of natural proteins while addressing their limitations—such as structural complexity, high production costs, and poor stability—artificial anion transporters have become one of central focuses in the field of artificial membrane transporters.[13–30] These synthetic systems open new avenues in both fundamental and applied research, demonstrating significant potential in treating anion transport-related disorders, designing stimuli-responsive materials, constructing synthetic biological systems, developing anticancer therapeutics, and advancing industrial ion separation technologies.[31–35]

A common feature of natural anion transport proteins is their use of positively charged amino acid residues (e.g., Arg, Lys) to electrostatically complement anion charges, forming selective filters.[36] Inspired by this, researchers have incorporated cationic groups (e.g., ammonium,[37–41] pyrrolinium,[42–43] imidazolium[44–46]) into artificial channels or carriers to reduce the energy barrier for anion transport and enhance selectivity through strategic charge distribution. However, such systems often suffer from pH sensitivity and chemical instability.

The σ-hole—a region of positive electrostatic potential along the covalent bond axis of certain atoms (e.g., halogens, sulfur, and phosphorus)—was first proposed by Brinck, Murray, and Politzer.[47] This feature enables directional interactions with electronegative species and offers several advantages in anion transport, including pH stability, strong directionality, tunable lipophilicity, and enhanced selectivity. To date, a series of anion transporters based on halogen bonds,[48–51] chalcogen bonds,[52–56] and pnictogen bonds[57–61] have been developed. Among these, Group 15 elements are particularly attractive due to their possession of three σ-holes

[*] Dr. F. Gou⁺, Q. Wang, Z. Yang, X. Yuan, Dr. W. Chang, Prof. Dr. J. Shen, Prof. Dr. H. Zeng
College of Chemistry, Fuzhou University, Fuzhou, Fujian 350116, China
E-mail: shenjie@fzu.edu.cn
hqzeng@fzu.edu.cn

X. Huangfu⁺, Prof. Dr. W.-X. Zhang
College of Chemistry and Molecular Engineering, Peking University, Haidian District, Beijing 100084, China
E-mail: wx_zhang@pku.edu.cn

[⁺] Both authors contributed equally to this work.

Additional supporting information can be found online in the Supporting Information section

and variable oxidation states, which enable fine-tuning of anion transport properties.[57] Current research has primarily focused on antimony- and bismuth-based anion carriers.[57–61]

Triphenylphosphonium (TPP^+), a classic mitochondria-targeting moiety, is widely used in diagnostics, therapy and drug delivery.[62–63] However, TPP^+ has traditionally been considered to possess insufficient σ-hole strength for effective anion recognition, due to delocalization of its positive charge into the adjacent benzene rings. To date, no anion transport activity has been reported using the TPP^+ or tetraphenylphosphonium scaffolds, and the development of efficient phosphorus-based σ-hole transporters remains an elusive frontier in the field of biomimetic membrane transport.

Although phosphorus atom exhibits a comparatively weaker σ-hole, its moderate binding strength may facilitate faster anion release. Moreover, its significantly lower biotoxicity relative to antimony or bismuth enhances its suitability for biomedical applications.[64]

We hypothesized that incorporating flexible aliphatic CH_2 spacers, as found in the tetrabenzylphosphonium framework (**1**–**5**, Figure 1a), would confer three key advantages to enhance the otherwise weak anion transport activity: (1) markedly minimizing conjugation-induced charge delocalization into the benzene rings as found in **6** and **7**, thereby concentrating nearly all the positive charge on the phosphorus atom to strengthen σ-hole strength and its electrostatic interactions with anions; (2) enabling H-atoms from both the CH_2 unit and benzene ring from the benzyl group to cooperatively participate in the formation of multiple H—bonds; and (3) increasing CH_2-mediated rotational freedom, likely promoting efficient molecular self-assembly and favorable σ-hole–anion alignment.

Here, we report that replacing phenyl groups with benzyl groups yields the first examples of phosphorus-based σ-hole/multihydrogen bond synergistic anion channels derived from the tetrabenzylphosphonium scaffold. These channels also represent the first mitochondria-targeting anion channels with potent cancer cell-killing activity, distinguishing them from Gale's first-in-class organelle-targeting anion carriers.[65] Furthermore, unlike Gale's carriers, which relies on two separate functional units—one for organelle targeting and another for anion transport—our dual-function organelle-targeting channels seamlessly integrate both capabilities within a single functional motif. Among the series, the top-performing channel **5** exhibits potent anticancer activity, with IC_{50} values as low as 1.4, 2.2, and 3.04 μM against HepG2, MDA-MB-231, and NCI-H1299 cells, respectively.

As shown in Figure 1a, we designed and evaluated five tetrabenzylphosphonium bromides (**1**–**5**), bearing different substituents. These compounds were synthesized following previously reported methods.[66] For comparison, we included control molecules **6** and **7**, which lack CH_2 units, and **8**, which likely lacks the ability to form a three-dimensional porous structure. We envisioned that molecules **1**–**5** could assemble into a 3D porous structure to facilitate transmembrane anion transport (Figure 1b).

High-quality colorless single crystals for **3** and **5** were obtained by slow evaporation of their $CHCl_3$ solutions over the course of a few days (for crystallographic data, see Table S1).[67] In the crystal structure, the presence of four tetrahedrally arranged relatively rigid benzyl groups enables molecules **3** and **5** to self-assemble into 3D porous frameworks, forming Br^--containing channels (Figures 1c,d, S1 and S2). Similarly, molecules of **6** also pack into a 3D porous structure, with Br^- ions enclosed within the channels (Figures 1e and S1c).[68]

A detailed analysis of the noncovalent interactions between the Br^- anion and surrounding molecules of **3**, **5,** or **6** in the solid state reveals distinctive features that support our hypothesis. Specifically, the Br^- anion forms a greater number of shorter noncovalent interactions with two molecules of **3** or three molecules of **5** than with four molecules of **6** (Figure 1f–h). In particular, the C—H···Br^- H—bonds and P^+···Br^- contacts in $(\mathbf{3})_2$•Br^- and $(\mathbf{5})_3$•Br^- range from 2.43 to 3.56 and 4.02 to 5.43 Å, respectively. In contrast, the corresponding distances in $(\mathbf{6})_4$•Br^- exceed 3.56 Å or measure 6.24 Å, respectively, indicating significantly weaker interactions.

At the B3LYP-D3/6–31G(d) level of theory, the H—bonds and ion-pair interactions collectively yield substantial binding energies of −165.3 and −137.9 kcal mol^{-1} for **3** and **5**, respectively, which are markedly greater than both the −76.3 kcal mol^{-1} calculated for **6** and the hydration energy of around −80 kcal mol^{-1} for bromide ion. These pronounced differences in binding energy imply that **3** and **5** are likely to display greater anion transport activity than **6**.

^{1}H NMR titration experiments, in which up to 30 equiv. of TBACl were added to a 0.5 mM solution of **4** in $CDCl_3$, reveal downfield shifts of 0.027 ppm for the benzyl protons and 0.018 ppm for one of the aromatic protons (Figure S5). These shifts suggest the involvement of multiple C—H···Cl^- H—bonding interactions in binding the chloride ions by **4**.

Prompted by these computational and titration results, we investigated the ion transport activities of **1–8** using a vesicle-based kinetic HPTS (8-hydroxypyrene-1,3,6-trisulfonic acid trisodium salt) assay, which employs the pH-sensitive HPTS dye encapsulated within DOPC (dioleoyl phosphatidylcholine)-based LUVs (large unilamellar vesicles, Figure 2a). The normalized fluorescence intensity data clearly demonstrate that tetrabenzylphosphonium compounds **1**–**5** possess enhanced ion transport capabilities relative to tetraphenylphosphonium compounds **6**–**8**. This underscores the pivotal role of the benzyl motif in strengthening intermolecular interactions with anions and promoting the formation of a three-dimensional porous network conducive to efficient ion translocation. Notably, compounds **4** and **5** exhibit the highest transport activities, reaching 82% and 81%, respectively, while chlorine-substituted **3** shows moderate activity at 59%.

Aside from the Cl^-/OH^- antiport mechanism illustrated in Figure 2a, other transport pathways and ionic species—such as Na^+/H^+ antiport, Na^+/OH^- symport and Cl^-/H^+ symport—-may also contribute to the observed enhancement in fluorescence intensity. To elucidate the most likely transport mechanism and species, we performed two lipid bilayer experiments. First, the Cl^--sensitive SPQ ((6-methoxy-N-(3-sulfopropyl))quinolinium) assay was performed to determine

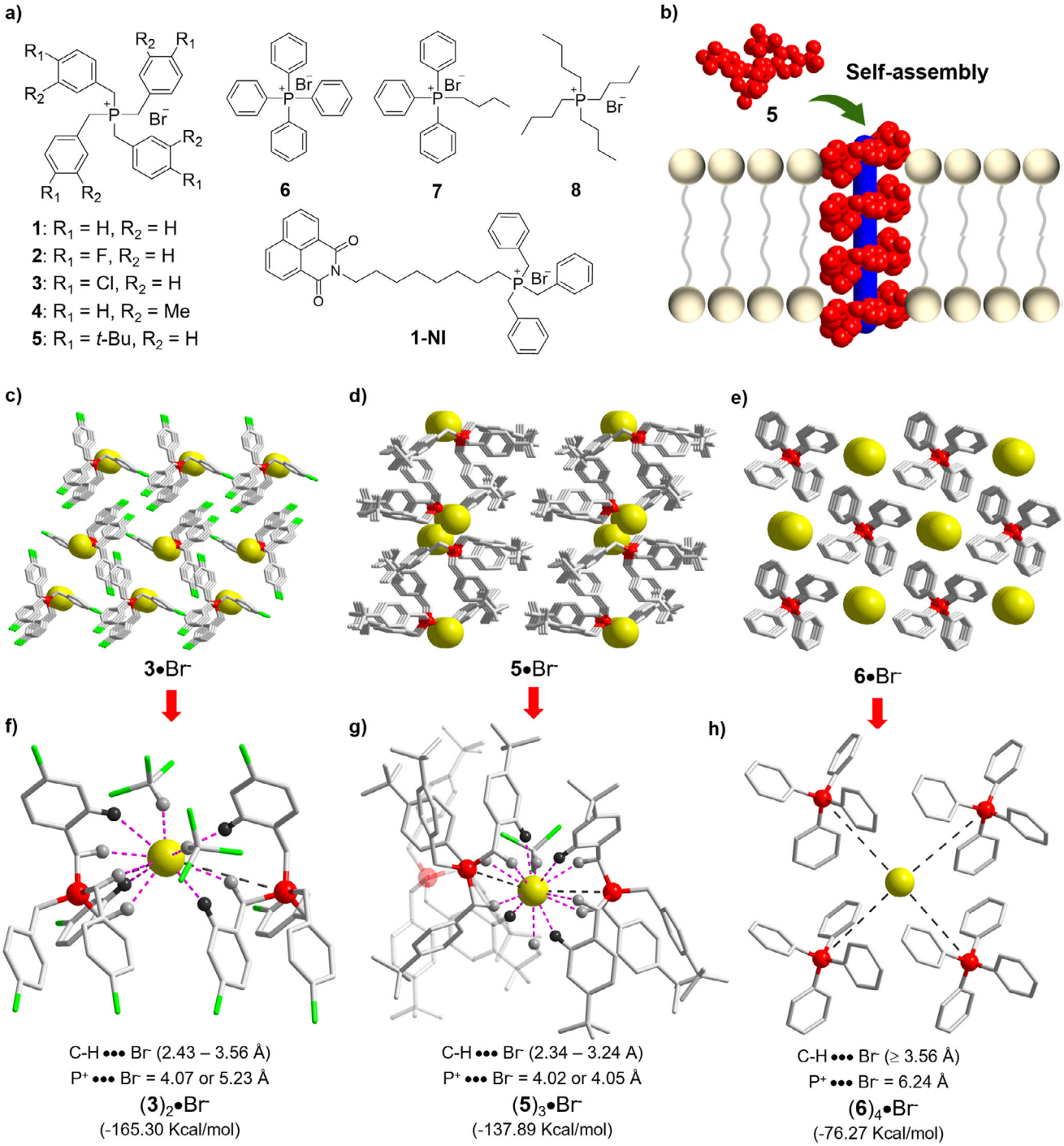

Figure 1. a) Chemical structures of anion-transporting tetrabenzylphosphonium bromides (**1–5**) and control compounds (**6–8**) that lack anion transport ability. b) Schematic illustration of the self-assembly of **5** within the bilayer membrane, forming a transmembrane pathway for facilitated anion transport. c–e) illustrates crystal structures of **3**•Br^-, **5**•Br^-, and **6**•Br^-. f–h) shows that, in the crystal structures, every Br^- anion interacts with two, three, and four cationic phosphorus centers as seen in(**3**)$_2$•Br^-, (**5**)$_3$•Br^-, and (**6**)$_4$•Br^-, with the C—H···Br^- H—bonds and P+···Br^- distances found in (**3**)$_2$•Br^- and (**5**)$_3$•Br^-) much shorter than those found in (**6**)$_4$•Br^-. Consequently, the binding energies for the crystal lattice to stabilize the Br^- anion are −165.30 kcal^{-1}mol for (**3**)$_2$ and −137.89 kcal mol^{-1} for (**5**)$_3$, values that are markedly higher than −76.27 kcal mol^{-1} calculated for (**6**)$_4$. All structural optimizations and energy calculations were performed at the level of B3LYP-D3/6–31G(d).

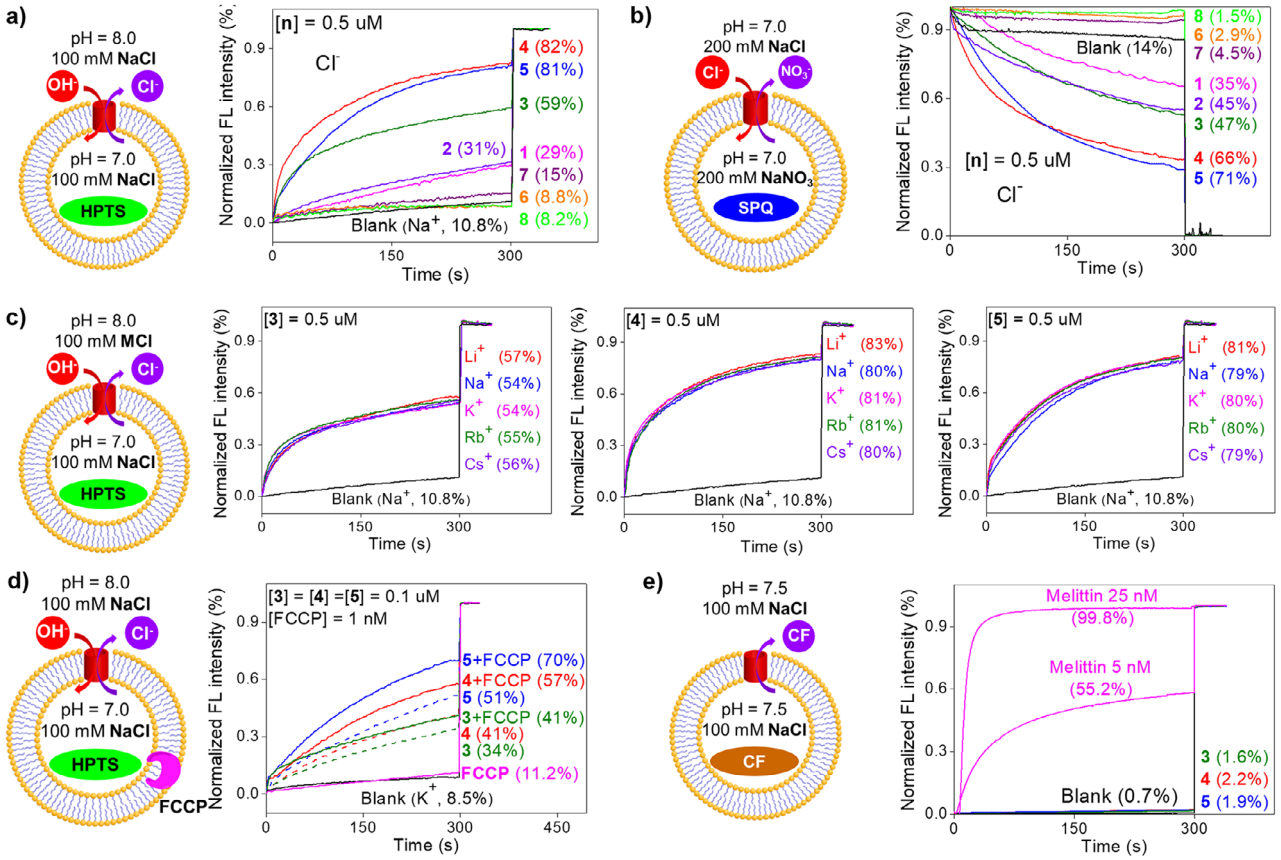

Figure 2. Transmembrane transport activity and mechanism study of **1–8**. a) Ion transport activities of **1–8** are evaluated using a DOPC-based pH-sensitive HTPS assay over a 5-min duration at 0.5 μM. b) The chloride-sensitive SPQ assay for evaluating the anion transport ability of **1–8**. c) The HPTS assay for ion transport study of **3–5**, employing different extravesicular salts (MCl, where M = Li, Na, K, Rb, and Cs) to evaluate cation transport activities. d) The HPTS assay using a proton carrier FCCP to compare the transport rate between H^+ and Cl^- mediated by **3–5** at 0.5 μM. e) CF dye leakage assay to confirm the membrane integrity in the presence of **3–5**. [Total lipid] = 97.5 μM.

whether chloride ions were being transported (Figure 2b). SPQ, a chloride-sensitive dye, exhibits fluorescence quenching in the presence of Cl^- ions. Using this assay, we observed that compounds **1–5** induce varying degrees of fluorescence quenching, with **4** and **5** showing the most pronounced effects at 66% and 71%, respectively. These results confirm the ability of **4** and **5** to facilitate efficient Cl^- transport. Conversely, **6–8** exhibit negligible changes in fluorescence, indicating minimal or no Cl^- transport activity. Second, the HPTS-based assays conducted with different extravesicular MCl salts (M = Li, Na, K, Rb, and Cs) reveal insignificant differences in ion transport activity (Figure 2c), suggesting that the observed anion transport is not strongly dependent on the nature of the accompanying cation. Together, these two lines of evidence exclude the involvement of Na^+/OH^- symport and Na^+/H^+ antiport ion transport mechanisms. Accordingly, the predominant ion transport pathway is either Cl^-/H^+ symport or Cl^-/OH^- antiport. Using a similar HPTS assay (Figure S7), we found both **3** and **5** transport ClO_4^-, NO_3^-, and Br^- more efficiently than Cl^-.

To compare the relative transport rate between Cl^- and H^+/OH^-, a highly active proton transporter FCCP (carbonyl cyanide 4-(trifluoromethoxy)phenylhydrazone) was introduced in the HPTS assay (Figure 2d). It should be noted that the FCCP experiment can't be used to verify either Cl^-/H^+ symport or Cl^-/OH^- antiport mechanisms since H^+ and OH^- can't be differentiated. In this assay, if H^+ or OH^- transport either through passive transport or channels was the slower step, FCCP—by accelerating H^+ movement—should alleviate this rate-limiting rate, leading to a significant enhancement in fluorescence intensity. After subtracting the baseline activities of FCCP alone and in its absence, an increase in transport efficiency by 4–14% for compounds **3–5** in the presence of FCCP therefore suggests a synergistic effect between compounds **3–5** and FCCP activity. Nevertheless, such a modest increase indicates that Cl^- transport may be not that much faster than H^+ or OH^-. Hill analyses of transport data gave the EC_{50} values of 0.17 μM or 0.17 mol% relative to lipids for **4** (Figure S8a) and 0.12 μM for **5** (Figure S8b), respectively, confirming high Cl^- transport activities.

We further conducted a CF (5(6)-carboxyfluorescein) leakage assay to evaluate the LUV membrane integrity in the presence of **3–5**. As shown in Figure 2e, 3–5 at 0.5 μM do not induce any measurable increase in fluorescence, indicating no CF dye leakage or membrane destruction. By comparison, melittin—a pore-forming peptide—induces substantial fluorescence increases of 55% and 100% at even lower concentrations of 5 and 25 nM, respectively.

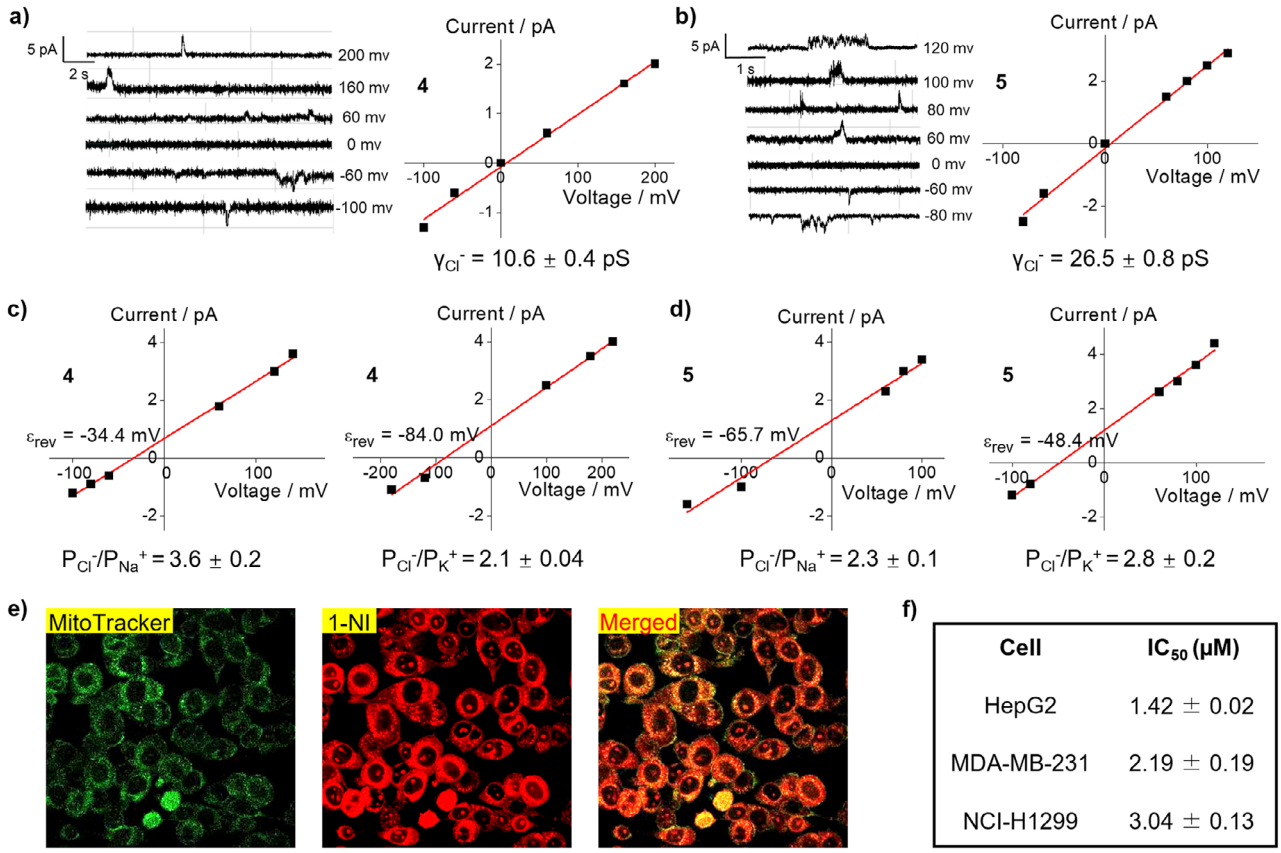

Cell	IC_{50} (μM)
HepG2	1.42 ± 0.02
MDA-MB-231	2.19 ± 0.19
NCI-H1299	3.04 ± 0.13

Figure 3. a) and b) present single channel current traces and current–voltage (I–V) curves (cis chamber = trans chamber = 1 M NaCl) from which chloride conduction rates (γCl^-) for **4** and **5** were determined to be 10.6 ± 0.4 and 26.5 ± 0.8 pS, respectively. c) and d) show I–V curves (cis chamber = 0.5 M NaCl or 0.5 M KCl, trans chamber = 1 M NaCl or 1 M KCl) from which the permeability ratios of $PCl^-/PNa^+$and PCl^-/PK^+ for **4** and **5** were determined. e) Colocalization of MitoTracker Red and **1-NI** fluorescence in 4T1 cells: 4T1 cells were treated with 8 μM **1-NI** for 12 h, followed by staining with MitoTracker Red and finally by capturing and merging the images using ImageJ (version 1.8.1) to assess colocalization of the red and blue signals. f) IC50 values (μM) for **5** against HepG2, MDA-MB-231, and NCI-H1299 cancer cells. For equations used for calculations of γCl^- and selectivity, see Supporting Information. All single channel current traces were measured in a diPhyPC-based bilayer membrane.

These results unequivocally confirm that the integrity of the LUV membrane is preserved in the presence of these compounds, and that the observed ion transport activities are not attributable to membrane-disruptive effects of the tetrabenzylphosphonium derivatives.

Single-channel electrophysiological experiments were performed for **4** and **5** in diPhyPC (1,2-diphytanoyl-sn-glycero-3-phosphocholine)-based planar lipid bilayer membrane using a planar lipid bilayer workstation (Figures 3a,b and S9). Consistent with expectations, both **4** and **5** display characteristic square-shaped signals, confirming that Cl^- transport proceeds through a channel mechanism. Based on the plotted I–V curves, the chloride conductance rates (γ_{Cl^-}) for **4** and **5** were calculated to be 10.6 ± 0.4 and 26.5 ± 0.8 pS, respectively, indicating their high efficiency in Cl^- transport.

The Cl^-/Na^+ and Cl^-/K^+ transport selectivity (P_{Cl^-}/P_{M^+}) for **4** and **5** was determined using single-channel conductance measurements under asymmetric conditions, with the *cis* chamber containing 0.5 M MCl and the *trans* chamber 1.0 M MCl (M = Na or K, Figures S10–S13). From the plotted I–V curves for **4** (Figure 3c), the reversal potentials were determined to be −34.4 and −84.0 mV under NaCl and KCl gradients, respectively. Based on these values, the Cl^-/Na^+ and Cl^-/K^+ selectivity factors were calculated to be 3.6 and 2.1, respectively, indicating a preferential transport of Cl^- over Na^+ and K^+. Similarly, for **5**, the Cl^-/Na^+ and Cl^-/K^+ selectivity factors were determined to be 2.3 and 2.8, respectively (Figure 3d).

To validate the intrinsic mitochondria-targeting capability of these cationic tetrabenzylphosphonium derivatives, compound **1** was conjugated with a naphthalimide moiety to yield a fluorescent probe, designated as **1-NI** (Figure 1a and Scheme S1). 4T1 cells were then co-incubated with **1-NI** and the commercially available mitochondrial dye MitoTracker Red. Fluorescence imaging reveal a strong colocalization between the green fluorescence of **1-NI** and the red signal from MitoTracker, resulting in a merged pink fluorescence in the cells (Figure 3e) and a Pearson's correlation coefficient value of 0.83. These findings confirm the selective and nearly exclusive mitochondrial localization of **1-NI**, attributed to the targeting ability of the cationic tetrabenzylphosphonium group.

Given that transmembrane Cl^- transport can induce apoptosis by disrupting cellular ion homeostasis, it is anticipated that these self-assembled Cl^--transporting channels

may exert cytotoxic effects on cancer cells.[35,51,69] To explore this potential, **5** was selected for evaluation of its anticancer activity against several common cancer cell lines, including HepG2, MDA-MB-231, and NCI-H1299. As summarized in Figure 3f and S14, the results reveal potent cytotoxicity, with IC_{50} values of 1.42, 2.19, and 3.04 μM, respectively—comparable to those of established chemotherapeutic agents such as doxorubicin (IC_{50} = 1.5 μM for HepG2) and paclitaxel (IC_{50} = 8.2 μM for HepG2).[70]

Through a strategically devised approach that transforms intrinsically weak anion transporters into highly potent ones, we have developed a novel class of unconventional artificial anion channel systems based on the self-assembly of quaternary tetrabenzylphosphonium salts. Crystal structure and computational analyses reveal that the benzyl groups in the structure not only give rise to a supporting three-dimensional porous architecture but also facilitate stronger intermolecular hydrogen bonding and ion-pair interactions with anions than their phenyl counterparts, resulting in markedly enhanced anion-binding affinity. Notably, the alkyl-substituted tetrabenzylphosphonium derivatives **4** and **5** exhibit higher anion transport activities, highlighting the importance of a more spacious three-dimensional porous framework that supports transmembrane anion transport via a channel mechanism. Beyond their transport properties, these quaternary phosphonium salts possess intrinsic and robust mitochondrial-targeting capabilities, ensuring precise and spatially predominant distribution at the subcellular level. Furthermore, this compound series shows promising anticancer potential, as exemplified by **5**, which exhibits IC_{50} values of 1.42–3.04 μM against three cancer cells—comparable to conventional chemotherapeutics—underscoring its potential for cancer treatment applications. This study represents the first demonstration of phosphorus-based σ-hole anion channels with intrinsic mitochondria-targeting capabilities, offering a promising platform for therapeutic applications.

Acknowledgements

This work is supported by the National Natural Science Foundation of China (22371048, 22271049, 21602055 and 22131001), the "Chu Ying Program" for the Top Yong Talents of Fujian Province, and the Postdoctoral Fellowship Program of CPSF under Grant Number GZC20230455 and a start-up grant from Fuzhou University.

Conflict of Interests

The authors declare no conflict of interest.

Data Availability Statement

The data that support the findings of this study are available from the corresponding author upon reasonable request.

Keywords: Artificial anion channels · Chloride transport · Self-assembly · Supramolecular chemistry · Tetrabenzylphosphonium

[1] C. A. Hübner, T. J. Jentsch, *Hum. Mol. Genet.* **2002**, *11*, 2435–2445.
[2] X. Wu, E. N. W. Howe, P. A. Gale, *Acc. Chem. Res.* **2018**, *51*, 1870–1879.
[3] T. J. Jentsch, K. Steinmeyer, G. Schwarz, *Nature* **1990**, *348*, 510–514.
[4] K. Steinmeyer, C. Ortland, T. J. Jentsch, *Nature* **1991**, *354*, 301–304.
[5] T. J. Jentsch, M. Pusch, *Physiol. Rev.* **2018**, *98*, 1493–1590.
[6] A. Picollo, M. Pusch, *Nature* **2005**, *436*, 420–423.
[7] P. A. Gale, C. C. Tong, C. J. E. Haynes, O. Adeosun, D. E. Gross, E. Karnas, E. M. Sedenberg, R. Quesada, J. L. Sessler, *J. Am. Chem. Soc.* **2010**, *132*, 3240–3241.
[8] T. Arakawa, T. Kobayashi-Yurugi, Y. Alguel, H. Iwanari, H. Hatae, M. Iwata, Y. Abe, T. Hino, C. Ikeda-Suno, H. Kuma, D. Kang, T. Murata, T. Hamakubo, A. D. Cameron, T. Kobayashi, N. Hamasaki, S. Iwata, *Science* **2015**, *350*, 680–684.
[9] H. Valkenier, O. Akrawi, P. Jurček, K. Sleziaková, T. Lízal, K. Bartik, V. Šindelář, *Chem* **2019**, *5*, 429–444.
[10] R. Dutzler, *FEBS Lett.* **2004**, *564*, 229–233.
[11] E. Park, E. B. Campbell, R. MacKinnon, *Nature* **2017**, *541*, 500–505.
[12] J. J. Thomas, *J. Physiol* **2015**, *593*, 4091–4109.
[13] Z. Chen, X. Xie, C. Jia, Q. Zhong, Q. Zhang, D. Luo, Y. Cao, Y. Mu, C. Ren, *Angew. Chem. Int. Ed.* **2024**, *63*, e202318811.
[14] S. Chattopadhayay, K. V. Banzal, P. Talukdar, *Angew. Chem. Int. Ed.* **2025**, *64*, e202414354.
[15] T. Yan, J. Liu, *Angew. Chem. Int. Ed.* **2025**, *64*, e202416200.
[16] Y. Lin, B. Wu, Y. Zeng, H. Yuan, C. Ji, Z. Liu, Y. Sui, T. Yin, X. Kong, Y. Zhu, J. Chen, C. Lang, *Angew. Chem. Int. Ed.* **2024**, *63*, e202408558.
[17] H. Chen, Y. Liu, X. Cheng, S. Fang, Y. Sun, Z. Yang, W. Zheng, X. Ji, Z. Wu, *Angew. Chem. Int. Ed.* **2021**, *60*, 10833–10841.
[18] A. Mondal, S. N. Save, S. Sarkar, D. Mondal, J. Mondal, S. Sharma, P. Talukdar, *J. Am. Chem. Soc.* **2023**, *145*, 9737–9745.
[19] S. Deng, Z. Li, L. Yuan, H. Q. Zeng, *Molecules* **2024**, *29*, 1118.
[20] T. Saha, M. S. Hossain, D. Saha, M. Lahiri, P. Talukdar, J. Yang, G. Yu, J. L. Sessler, I. Shin, P. A. Gale, F. Huang, *J. Am. Chem.* **2021**, *7*, 3256–3291.
[21] L. Yuan, P. Jiang, J. Hu, H. Q. Zeng, Y. Huo, Z. Li, H. Q. Zeng, *Chin. Chem. Lett.* **2022**, *33*, 2026–2030.
[22] W.-L. Huang, X.-D. Wang, Y.-F. Ao, Q.-Q. Wang, D.-X. Wang, *J. Am. Chem. Soc.* **2020**, *142*, 13273–13277.
[23] R. Cao, R. B. Rossdeutcher, Y. Zhong, Y. Shen, D. P. Miller, T. A. Sobiech, X. Wu, L. S. Buitrago, K. Ramcharan, M. I. Gutay, M. F. Figueira, P. Luthra, E. Zurek, T. Szyperski, B. Button, Z. Shao, B. Gong, *Nat. Chem.* **2023**, *15*, 1559–1568.
[24] R. Ye, C. Ren, J. Shen, N. Li, F. Chen, A. Roy, H. Q. Zeng, *J. Am. Chem. Soc.* **2019**, *141*, 9788–9792.
[25] X. Wu, J. R. Small, A. Cataldo, A. M. Withecombe, P. Turner, P. A. Gale, *Angew. Chem. Int. Ed.* **2019**, *58*, 15142–15147.
[26] X. Li, B. Shen, X.-Q. Yao, D. Yang, *J. Am. Chem. Soc.* **2007**, *129*, 7264–7265.
[27] W.-L. Huang, X.-D. Wang, Y.-F. Ao, Q.-Q. Wang, D.-X. Wang, *Angew. Chem. Int. Ed.* **2023**, *62*, e202302198.
[28] P. H. Schlesinger, R. Ferdani, J. Liu, J. Pajewska, R. Pajewski, M. Saito, H. Shabany, G. W. Gokel, *J. Am. Chem. Soc.* **2002**, *124*, 1848–1849.

[29] N. Busschaert, M. Wenzel, M. E. Light, P. Iglesias-Hernández, R. Pérez-Tomás, P. A. Gale, *J. Am. Chem. Soc.* **2011**, *133*, 14136–14148.
[30] L. Yuan, J. Shen, R. Ye, F. Chen, H. Q. Zeng, *Chem. Commun.* **2019**, *55*, 4797–4800.
[31] P. R. Brotherhood, A. P. Davis, *Chem. Soc. Rev.* **2010**, *39*, 3633–3647.
[32] A. P. Davis, D. N. Sheppard, B. D. Smith, *Chem. Soc. Rev.* **2007**, *36*, 348–357.
[33] J. T. Davis, O. Okunola, R. Quesada, *Chem. Soc. Rev.* **2010**, *39*, 3843.
[34] P. A. Gale, J. T. Davis, R. Quesada, *Chem. Soc. Rev.* **2017**, *46*, 2497–2519.
[35] G. W. Gokel, S. Negin, *Acc. Chem. Res.* **2013**, *46*, 2824–2833.
[36] G. You, *Med. Res. Rev.* **2004**, *24*, 762–774.
[37] S. Otto, M. Osifchin, S. L. Regen, *J. Am. Chem. Soc.* **1999**, *121*, 7276–7277.
[38] N. Madhavan, E. C. Robert, M. S. Gin, *Angew. Chem. Int. Ed.* **2005**, *44*, 7584–7587.
[39] J. Kempf, A. Schmitzer, *RSC Adv.* **2016**, *6*, 42713–42719.
[40] C. Zhang, J. Tian, S. Qi, B. Yang, Z. Dong, *Nano Lett.* **2020**, *20*, 3627–3632.
[41] N. Akhtar, N. Pradhan, G. K. Barik, S. Chatterjee, S. Ghosh, A. Saha, P. Satpati, A. Bhattacharyya, M. K. Santra, D. Manna, *ACS Appl. Mater. Interfaces* **2020**, *12*, 25521–25533.
[42] B. Díaz de Greñu, P. I. Hernández, M. Espona, D. Quiñonero, M. E. Light, T. Torroba, R. Pérez-Tomás, R. Quesada, *Chem.-Eur. J.* **2011**, *17*, 14074–14083.
[43] E. Hernando, V. Capurro, C. Cossu, M. Fiore, M. García-Valverde, V. Soto-Cerrato, R. Pérez-Tomás, O. Moran, O. Zegarra-Moran, R. Quesada, *Sci. Rep.* **2018**, *8*, 2608.
[44] M. Vidal, A. Schmitzer, *Chem.-Eur. J.* **2014**, *20*, 9998–10004.
[45] J. Gravel, R. A. Schmitzer, *Supramol. Chem.* **2015**, *27*, 364–371.
[46] S.-P. Zheng, Y.-H. Li, J.-J. Jiang, A. van der Lee, D. Dumitrescu, M. Barboiu, *Angew. Chem. Int. Ed.* **2019**, *58*, 12037–12042.
[47] T. Brinck, J. S. Murray, P. Politzer, *Int. J. Quantum Chem.* **1992**, *44*, 57–64.
[48] A. V. Jentzsch, D. Emery, J. Mareda, S. K. Nayak, P. Metrangolo, G. Resnati, N. Sakai, S. Matile, *Nat. Commun.* **2012**, *3*, 905.
[49] A. Vargas Jentzsch, D. Emery, J. Mareda, P. Metrangolo, G. Resnati, S. Matile, *Angew. Chem. Int. Ed.* **2011**, *50*, 11675–11678.
[50] L. E. Bickerton, A. J. Sterling, P. D. Beer, F. Duarte, M. J. Langton, *Chem. Sci.* **2020**, *11*, 4722–4729.
[51] C. Ren, X. Ding, A. Roy, J. Shen, S. Zhou, F. Chen, S. F. Yau Li, H. Ren, Y. Y. Yang, H. Q. Zeng, *Chem. Sci.* **2018**, *9*, 4044–4051.
[52] L. E. Bickerton, A. Docker, A. J. Sterling, H. Kuhn, F. Duarte, P. D. Beer, M. J. Langton, *Chem.-Eur. J.* **2021**, *27*, 11738–11745.
[53] S. Benz, M. Macchione, Q. Verolet, J. Mareda, N. Sakai, S. Matile, *J. Am. Chem. Soc.* **2016**, *138*, 9093–9096.
[54] H. V. Humeniuk, A. Gini, X. Hao, F. Coelho, N. Sakai, S. Matile, *JACS Au.* **2021**, *1*, 1588–1593.
[55] A. Docker, T. G. Johnson, H. Kuhn, Z. Zhang, M. J. Langton, *J. Am. Chem. Soc.* **2023**, *145*, 2661–2668.
[56] B. Zhou, F. P. Gabbaï, *Chem. Sci.* **2020**, *11*, 7495–7500.
[57] L. M. Lee, M. Tsemperouli, A. I. Poblador-Bahamonde, S. Benz, N. Sakai, K. Sugihara, S. Matile, *J. Am. Chem. Soc.* **2019**, *141*, 810–814.
[58] G. Park, D. J. Brock, J.-P. Pellois, F. P. Gabbaï, *Chem* **2019**, *5*, 2215–2227.
[59] G. Park, F. P. Gabbaï, *Chem. Sci.* **2020**, *11*, 10107–10112.
[60] B. L. Murphy, F. P. Gabbaï, *J. Am. Chem. Soc.* **2024**, *146*, 7146–7151.
[61] N. H. Hunter, F. P. Gabbaï, *Angew. Chem. Int. Ed.* **2025**, *64*, e202414699.
[62] R. A. J. Smith, C. M. Porteous, A. M. Gane, M. P. Murphy, *Proc. Natl. Acad. Sci* **2003**, *100*, 5407–5412.
[63] D.-Y. Kim, H.-J. Kim, K.-H. Yu, J.-J. Min, *Bioconjugate Chem.* **2012**, *23*, 431–437.
[64] A. Singh, A. Torres-Huerta, F. Meyer, H. Valkenier, *Chem. Sci.* **2024**, *15*, 15006–15022.
[65] W. G. Ryder, A. Levina, M. E. Graziotto, B. A. Hawkins, D. E. Hibbs, E. J. New, P. A. Gale, *Chem* **2025**, *11*, 102247.
[66] X. Huangfu, W. Liu, H. Xu, Z. Wang, J. Wei, W.-X. Zhang, *Inorg. Chem.* **2023**, *62*, 12009–12017.
[67] The supplementary crystallographic data for this paper can be found under deposition numbers 2417178 (for 3) and 2417179 (for 5). These data are provided free of charge by the joint Cambridge Crystallographic Data Centre and Fachinformationszentrum Karlsruhe Access Structures service www.ccdc.cam.ac.uk/structures.
[68] CCDC 153818, see: A. L. Spek, *CSD Communication* **2000**, https://doi.org/10.5517/cc551w7.
[69] H. Gill, M. R. Gokel, M. McKeever, S. Negin, M. B. Patel, S. Yin, G. W. Gokel, *Coord. Chem. Rev.* **2020**, *412*, 213264.
[70] J. Shen, Y. Gu, L. Ke, Q. Zhang, Y. Cao, Y. Lin, Z. Wu, C. Wu, Y. Mu, Y.-L. Wu, C. Ren, H. Q. Zeng, *Nat. Commun.* **2022**,*13*, 5985.

Manuscript received: May 31, 2025
Revised manuscript received: June 27, 2025
Accepted manuscript online: July 03, 2025
Version of record online: July 16, 2025